SHOCK, Vol. 60, No. 5, pp. 698–706, 2023

OPEN

SEPSIS LEADS TO IMPAIRED MITOCHONDRIAL CALCIUM UPTAKE AND SKELETAL MUSCLE WEAKNESS BY REDUCING THE MICU1:MCU PROTEIN RATIO

Xuexin Li,*,† Bowen Sun,*,† Jie Li,*,† Wanlin Ye,‡ Mingjuan Li,*,† Fasheng Guan,*,† Songlin Wu,*,† Xuerong Luo,*,† Jianguo Feng,*,† Jing Jia,*,† Xueru Liu,*,† Tao Li,‡ and Li Liu*,†

**Department of Anesthesiology, The Affiliated Hospital of Southwest Medical University, Luzhou, Sichuan Province, China; †Anesthesiology and Critical Care Medicine Key Laboratory of Luzhou, Southwest Medical University, Luzhou, Sichuan Province, China; and ‡Laboratory of Mitochondria and Metabolism, West China Hospital of Sichuan University, Chengdu, China*

Received 2 May 2023; first review completed 23 May 2023; accepted in final form 29 Aug 2023

ABSTRACT—**Purpose:** Intensive care unit–acquired weakness (ICUAW) is a severe neuromuscular complication that frequently occurs in patients with sepsis. The precise molecular pathophysiology of mitochondrial calcium uptake 1 (MICU1) and mitochondrial calcium uniporter (MCU) in ICUAW has not been fully elucidated. Here, we speculate that ICUAW is associated with MICU1:MCU protein ratio–mediated mitochondrial calcium ($[Ca^{2+}]_m$) uptake dysfunction. **Methods:** Cecal ligation and perforation (CLP) was performed on C57BL/6J mice to induce sepsis. Sham-operated animals were used as controls. Lipopolysaccharide (LPS) (5 μg/mL) was used to induce inflammation in differentiated C2C12 myoblasts. Compound muscle action potential (CMAP) was detected using a biological signal acquisition system. Grip strength was measured using a grip-strength meter. Skeletal muscle inflammatory factors were detected using ELISA kits. The cross-sectional area (CSA) of the tibialis anterior (TA) muscle was detected by hematoxylin and eosin staining. Cytosolic calcium ($[Ca^{2+}]_c$) levels were measured using Fluo-4 AM. Adeno-associated virus (AAV) was injected into TA muscles for 4 weeks to overexpress MICU1 prophylactically. A lentivirus was used to infect C2C12 cells to increase MICU1 expression prophylactically. **Findings:** The results suggest that sepsis induces $[Ca^{2+}]_m$ uptake disorder by reducing the MICU1:MCU protein ratio, resulting in skeletal muscle weakness and muscle fiber atrophy. However, MICU1 prophylactic overexpression reversed these effects by increasing the MICU1:MCU protein ratio. **Conclusions:** ICUAW is associated with impaired $[Ca^{2+}]_m$ uptake caused by a decreased MICU1:MCU protein ratio. MICU1 overexpression improves sepsis-induced skeletal muscle weakness and atrophy by ameliorating the $[Ca^{2+}]_m$ uptake disorder.

KEYWORDS—Sepsis; ICUAW; MICU1; mitochondrial Ca^{2+} uniporter; calcium; muscle atrophy

INTRODUCTION

Intensive care unit–acquired weakness (ICUAW) is a severe neuromuscular complication that frequently occurs in patients with sepsis (1). Approximately 60%–100% of patients with sepsis will eventually develop ICUAW, which is characterized by decreased muscle strength that leads to persistent physical impairment (2,3). ICUAW has an incidence of 40%–46% (4). The underlying pathophysiological effects of ICUAW are complex and have not been fully clarified but include limited autophagy, mitochondrial dysfunction, inflammasome activation, cell death, and necroptosis (5–7). However, current literature indicates that the accumulation of injured mitochondria and depressed mitochondrial function are important triggers of ICUAW (8,9).

Mitochondria take up calcium *via* the mitochondrial calcium uniporter complex (mtCU) in response to increased cellular energy (10,11). Mitochondrial calcium uptake 1 (MICU1) resides in the mitochondrial intermembrane and monitors cytosolic calcium ($[Ca^{2+}]_c$) transients. It plays the role of a "gatekeeper" at low $[Ca^{2+}]_c$ levels while adopting a structural conformation conducive to Ca^{2+} inflow with mitochondrial calcium uptake 2 (MICU2) at high $[Ca^{2+}]_c$ levels by binding to Ca^{2+} (12,13). In addition, MICU1 protects against myocardial ischemia/reperfusion and diabetic cardiomyopathy (14). A lack of MICU1 leads to impaired mitochondrial calcium ($[Ca^{2+}]_m$) uptake during excitation-contraction coupling, which manifests as muscle atrophy and fatigue (15,16). In addition, mitochondrial calcium uniporter (MCU) and MICU1 show tissue-specific mRNA expression, and only the MICU1:MCU protein ratio shows a complementary pattern with $[Ca^{2+}]_m$ uptake (17–19). To the best of our knowledge, the role of the MICU1:MCU protein ratio in sepsis-induced skeletal muscle weakness has not yet been reported.

Based on the current theoretical framework, we hypothesized that sepsis decreases the MICU1:MCU protein ratio, leading to a disturbance in $[Ca^{2+}]_m$ uptake that results in muscle weakness and atrophy. Therefore, we aimed to investigate the role of the MICU1:MCU protein ratio in sepsis-induced muscle weakness by establishing a mouse model of sepsis and cellular inflammation models and exploring potential therapeutic targets for ICUAW.

MATERIALS AND METHODS

Animals and groups

Eight-week-old male C57BL/6J mice were purchased from Huafukang Biotechnology Co, Ltd (China) and raised in a 12-h light/dark environment. Forty

Address reprint requests to Tao Li, MD, PhD, Laboratory of Mitochondria and Metabolism, West China Hospital of Sichuan University, No. 37, Wainan Guoxue Road, Chengdu 610041, Sichuan province, China. E-mail: scutaoli1981@scu.edu.cn; Co-correspondence: Li Liu, MD, PhD, Department of Anesthesiology, The Affiliated Hospital of Southwest Medical University, No 25 Taiping street, Luzhou, Sichuan Province, 646000, China. E-mail: niuniudoctor@swmu.edu.cn

This study was supported by Sichuan Science and Technology Program 2022YFS0632.

Supplemental digital content is available for this article. Direct URL citation appears in the printed text and is provided in the HTML and PDF versions of this article on the journal's Web site (www.shockjournal.com).

DOI: 10.1097/SHK.0000000000002221

specific pathogen-free (SPF) mice were randomly divided into four groups: a sham operation group (Sham) and 6-, 12-, and 24-h cecal ligation and perforation (CLP) groups (CLP-6, CLP-12, and CLP-24 h). Another 20 six-week-old SPF mice were used for adeno-associated virus (AAV) infection of the tibialis anterior (TA) muscle for 4 weeks. The left TA muscle was transfected with an empty plasmid without the AAV target gene (groups labeled AAV-Control), and the contralateral TA muscle was transfected with the AAV target gene plasmid MICU1 to enhance MICU1 expression prophylactically (groups labeled AAV-MICU1). Mice were randomly divided into two groups: a sham group (AAV-C-Sham and AAV-M-Sham groups) and a CLP modeling group for 24 h (AAV-C-CLP and AAV-M-CLP groups).

Animal model of sepsis

CLP is the "gold standard" rodent model for abdominal sepsis (20,21). Briefly, mice were anesthetized with sodium pentobarbital (1%, 50 mg/kg intraperitoneally [i.p.]) and injected with buprenorphine (0.05 mg/kg i.p.) for analgesia. A 1-cm incision was made in the midline of the abdomen using surgical forceps and scissors. Half of the cecum was ligated with a 4-0 silk thread. A chosen needle was used to puncture the cecum, and stool was gently squeezed out. Only cecal exploration was performed in sham group (22). At the end of the procedure, the mice were resuscitated by a subcutaneous injection of Ringer's lactate solution (23). All animal procedures were approved by the Animal Ethics Committee of Southwest Medical University on January 2, 2022, and the number was SWMU20220085.

Cell culture and groups

Murine C2C12 myoblasts (iCell-m013) were grown in Dulbecco's Modified Eagle Medium (DMEM) with 10% fetal bovine serum, 100 U/mL penicillin, and 100 μg/mL streptomycin in a humidified incubator with 5% CO_2 at 37°C. C2C12 cells were grown to near confluence (90%) and transferred to DMEM containing 2% horse serum to induce cell differentiation for 5–6 days (24). In addition, 5 μg/mL of lipopolysaccharide (LPS) (O111:B4, Sigma-Aldrich) was used to induce inflammation in C2C12 myoblasts.

The cells were divided into four groups according to the experimental time point: control group (control) and 6-, 12-, and 24-h LPS intervention groups (LPS-6, LPS-12, and LPS-24 h). Similarly, lentivirus (LV)-infected cells carrying the MICU1 plasmid of interest were used to increase MICU1 expression prophylactically (labeled the LV-MICU1 group), and LV-infected cells carrying empty plasmids were used as the control group (LV-Control group). Subsequently, the cells were divided into control (LV-C-Control and LV-M-Control groups) and LPS intervention groups for 24 h (LV-C-LPS and LV-M-LPS groups).

Animal plasma IL-6 and TNF-α measurements

Five mice from each group were randomly selected after CLP modeling. All mice in all groups were anesthetized with 1% sodium pentobarbital. Blood samples were gathered *via* cardiac puncture and centrifuged at 12,000 rpm for 15 min at 4°C. IL-6 and TNF-α concentrations in the culture supernatant and plasma were determined using mouse ELISA kits (MEIMIAN, China) according to the manufacturer's protocol.

Compound muscle action potential

The compound muscle action potential (CMAP) test is an appropriate and sensitive method for evaluating neuromuscular function in mice (25). First, the temperature of each mouse was maintained at approximately 37°C with a heating light, and the hind leg was fixed on an operating table with duct tape after anesthesia administration. Stimulation electrodes were placed on both sides of the sciatic nerve, and the needle was pushed vertically 5 mm subcutaneously, with a distance of approximately 2 cm between the electrodes. The recording electrode was placed subcutaneously to align the gastrocnemius muscle. The reference electrode was inserted subcutaneously next to the Achilles tendon in the direction of 30°, with 2–5 mm of the needle under the skin (26). The amplitude, duration, and latency of CMAP were tested as the primary parameters.

Grip strength test

The noninvasive grip test was used to assess the strength of the mice and identify neuromuscular disorders (27). The mice used their front paws to grab a horizontal bar attached to the gauge, and their tails were slowly pulled back for 2–3 s by an experienced investigator. The peak tension was automatically recorded when the mouse released the bar. Five grip strength measurements were taken at each time point, and the average result was used for analysis. The percentage of grip strength drop before and after modeling was used to assess changes in mouse grip strength. Grip strength was normalized to concomitant body weight, and low grip strength indicated weak muscle strength (28).

Histology and morphometric analysis

The TA muscles were harvested, fixed with 4% paraformaldehyde for 12 h, and transferred to 20% sucrose overnight. Then, 4-μm-thick transverse sections of the TA muscle were stained with hematoxylin and eosin (H&E) to assess muscle morphology. For quantitative analysis, images were acquired using an optical microscope (KFBIO, China). Analyses were performed using ImageJ Pro software on a minimum of four randomly selected images of the TA muscle. Each image had an average of 60 muscle fibers.

Intramuscular AAV injections

The tri-plasmid AAV2/9 system (carrier plasmid carrying the gene of interest or shRNA, pAAV-RC, or pHelper vector plasmid) was visually packaged. As previously described (29), the viral genome was copied with a titer of 1.3×10^{12} vg/mL into the TA muscles of the mice under general anesthesia (2% isoflurane) and had multipoint injections for a total of 24 μL.

A contralateral leg injection design was used. A plasmid loaded with the gene of interest (AAV-MICU1) was injected into the right TA muscle of the mice, and an equal amount of an empty transgenic carrier plasmid (AAV-shRNA) was injected into the contralateral TA muscle as a paired control. Four weeks later, CLP was performed to establish sepsis models. AAV was purchased from HanBio (HH20220303CD, China), and the animal studies were approved by an external ethics committee.

LV infection

Viral packaging was performed using a tri-plasmid lentiviral system, including vector plasmids carrying the gene of interest, or shRNA, and virus-packed helper plasmids, psPAX2 and pMD2G vectors. LV was purchased from HanBio (HH20220316CD, China). The MICU1 plasmid of interest was cloned into LV vectors and overexpressed in C2C12 cells. An empty carrier plasmid carrying shRNA was used as the negative control.

According to the manufacturer's instructions, the cells were seeded at a density of 2,000 cells/cm^2 to infect the viruses. The next day, the expressing LV was diluted in a cell culture medium supplemented with 5 μg/mL polybrene (YEASEN, China) for transduction. Viruses were removed 24 h after infection, and fresh cell medium supplemented with 2 μg/mL puromycin (YEASEN, China) was added. After 5 days, transduced puromycin-resistant cells were selected for further processing.

Evaluation of mitochondrial calcium uptake and efflux

After 5 days of C2C12 cell differentiation, cells were treated with 1 μM Thapsigargin (Tg) (T9033, Sigma-Aldrich) for 10 min at 37°C. Tg is a blocker of sarco/endoplasmic reticulum Ca^{2+}-ATPase. Phenol red-free medium was used, and 1 μM Fluo-4 AM (F14217, Thermo Fisher) was loaded to detect $[Ca^{2+}]_c$, whereas Pluronic F-127 (Solarbio, China) was added to improve the cell permeability of the dye. The cells were incubated at 37°C for 20 min before removing Fluo-4 AM.

At an excitation wavelength of 494 nm and an emission wavelength of 506 nm, the fluorescence signal after Fluo-4 AM binding to calcium ions was monitored to detect $[Ca^{2+}]_c$. At 60 s, different concentrations of Ca^{2+} (2.5 and 20 μM) were added for the experiment requirements.

The clearance of extramitochondrial Ca^{2+} was representative of $[Ca^{2+}]_m$ uptake. At 420 s, 10 μM of Na^+-Ca^{2+} exchange inhibitor (CGP-37157, ab120012, Abcam) was added to block the efflux of $[Ca^{2+}]_m$. At 780 s, 10 μM of an MCU inhibitor (Ru360, HY-122898, MedChemExpress) was added to inhibit $[Ca^{2+}]_m$ uptake. Finally, at 900 s, carbonyl cyanide-*p*-trifluoromethoxyphenylhydrazone (FCCP, HY-100410, MedChemExpress) was added, and the assay was terminated after 2 min. The role of FCCP was to depolarize the inner mitochondrial membrane and confirm that high levels of $[Ca^{2+}]_c$ originated from $[Ca^{2+}]_m$ (30). All experiments were performed at 37°C and recorded using Cytation 5 (Biotek, USA) (31).

Immunoblotting

Frozen TA muscle samples (30–40 g) were homogenized in an ice-cold lysis buffer. The muscle homogenates were kept on ice for 40 min with periodic agitation and then centrifuged at 12,000 rpm for 15 min at 4°C. The supernatants were collected, and the pellets were discarded. The protein content of each sample was determined using a BCA assay kit (Beyotime, China). Protein samples were separated by SDS-PAGE and transferred to NC membranes in a wet transblot system. After blocking with 5% skimmed milk, they were blotted with the following primary antibodies: MICU1 (ab190114, Abcam, 1:1,000), MICU2 (ab101465, Abcam, 1:1,200), MCU (14,997 s, Cell Signaling Technology, 1:1,000), essential MCU regulator (EMRE) (ab157387, Abcam, 1:1,200), muscle RING-finger containing protein 1 (MuRF1, sc-398,608, Santa Cruz, 1:1,200), muscle atrophy Fbox protein (MAFbx, sc-166,806, Santa Cruz, 1:1,200), and GAPDH (sc-32,233, Santa Cruz, 1:1,000) at 4°C overnight. On the second day, membranes were

Table 1. **Primers are used for real-time polymerase chain reaction experiments to detect the expression of various genes**

Gene	Forward primer	Reverse primer
MICU1	5′-CTTGGAGAGTGTGGGCTCAT-3′	5′-ATGTCTACCTCTCCGTCTCCA-3′
MICU2	5′-AGACTTTGCAGAATGGCTACT-3′	5′-ACAGGGCGATGAGCTAAACT-3′
MCU	5′-GATGACGTGACGGTGGTTTA-3′	5′-GTCAGAGATAGGCTTGAGTGTG-3′
EMRE	5′-ACTCCCAGTCCAGAAACCAC-3′	5′-ACTCCTTGTTCTTCCGACACTT-3′
MuRF1	5′-AGAAGTCGGGGGTCAGGGGACG-3′	5′-GGTCCATGATCACTTCATGGCGGCACGAGG-3′
MAFbx	5′-ATGCACACTGGTGCAGAGAG-3′	5′-TGTAAGCACACAGGCAGGTC-3′
GAPDH	5′-GGTTGTCTCCTGCGACTTCA-3′	5′-CCCTGTTGCTGTAGCCGTAT-3′

incubated with the corresponding secondary antibodies at room temperature for 1 h. Immunoreactive bands were visualized and analyzed using ImageJ software.

Quantitative real-time PCR

Total RNA was isolated using TRIzol reagent (TIANGEN, China) and reverse transcribed using HiScript RT SuperMix (Vazyme, China) (32). Quantitative real-time polymerase chain reaction (qRT-PCR) was performed using the CFX Connect Real-Time PCR System (CFX Manager, USA). The specific primer groups shown in Table 1 were used to quantify the mRNA expression levels.

Statistical analysis

All experiments were performed independently and included at least three biological replicates. All statistical analyses were performed using GraphPad Prime 9, and values were expressed as mean ± SEM. Comparisons between two groups were performed using two-tailed Student's *t* tests. Differences among at least three groups were analyzed using ANOVA, and variables across groups treated with different operations were compared using a post hoc test (Tukey's test). Correlation analysis was performed using Pearson product-moment correlation. The level of significance was set at 0.05.

RESULTS

Sepsis-induced impairment of neuromuscular function and skeletal muscle atrophy

To explore the effects of sepsis on muscle function, we examined the CMAP and grip strength of the mice. The results (Figs. 1A–1D) show that the amplitude of CMAP decreased compared with that in the control group, and the duration and latency increased, especially at 24 h, in the CLP group ($P < 0.05$). The grip strength test was performed to assess muscle weakness. We found that grip strength began to decrease at CLP-6 h and decreased by up to nearly 70% at CLP-24 h ($P < 0.05$, Fig. 1E). We further analyzed whether sepsis induces skeletal muscle atrophy by measuring the cross-sectional area (CSA) of the TA muscles and the expression levels of atrophy-related ubiquitin ligases (MuRF1 and MAFbx). The results showed that the CSA of the TA muscles in the CLP group decreased ($P < 0.05$, Figs. 1F–1G), and MuRF1 and MAFbx expression increased ($P < 0.05$, Figs. 1H–1J).

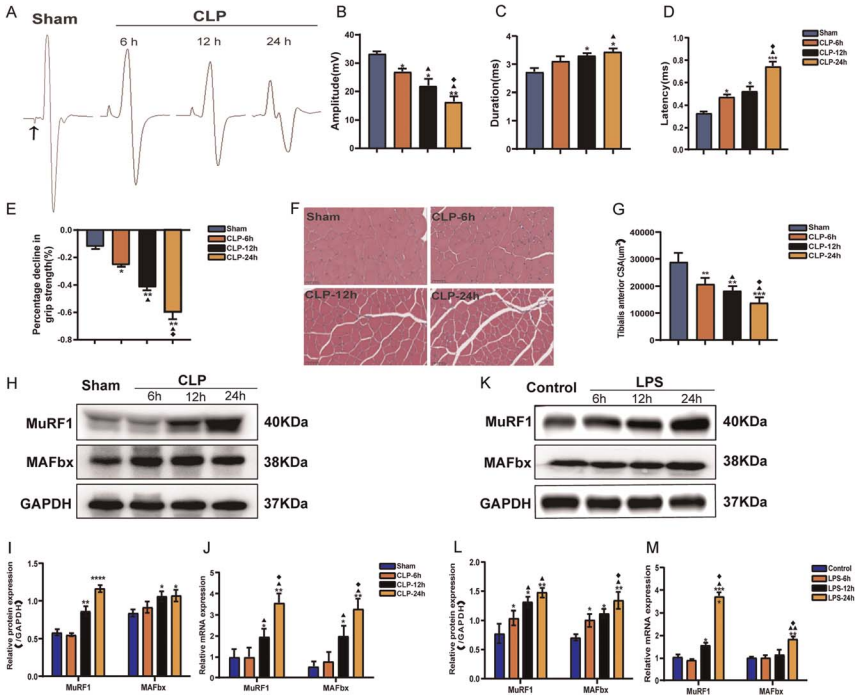

Fig. 1. **Neuromuscular function and skeletal muscle atrophy in mice after cecal ligation and puncture (CLP) modeling.** (A–D) Representative images of compound muscle action potential (CMAP) in each group along with three main parameters: amplitude, duration, and latency, $n = 5$. (E) Percentage decline in grip strength after CLP modeling in mice, $n = 5$. (F–G) Representative hematoxylin and eosin–stained tibialis anterior (TA) muscles (scale bar = 50 μm) and cross-sectional areas of TA muscles, $n = 5$. (H–J) After mice CLP modeling, the expression levels of MuRF1 and MAFbx were detected by Western blotting and quantitative polymerase chain reaction (qPCR) methods, $n = 3$. (K–M) After intervention with 5 μg/mL LPS, C2C12 cells were detected with Western blotting and qPCR methods to detect the expression levels of MuRF1 and MAFbx, $n = 3$. Data are shown as mean ± SEM. $^{*}P < 0.05$ compared with the sham group (control group), $^{\blacktriangle}P < 0.05$ compared with the 6-hour intervention group, and $^{\bullet}P < 0.05$ compared with the 12-hour intervention group.

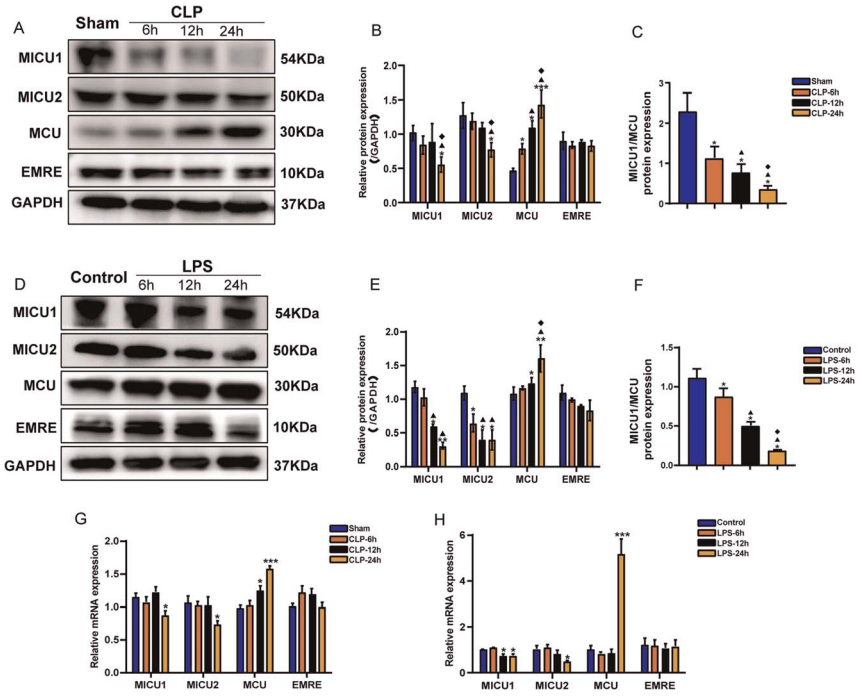

FIG. 2. **Effects of sepsis on the composition of the mitochondrial calcium uniporter complex (mtCU) in animal and cellular experiments.** (A–B) Western blotting analysis of the effects of CLP modeling on MICU1, MICU2, MCU, EMRE, and GAPDH in mice tibialis anterior (TA) muscles, $n = 3$. (C) Effects of sepsis on the MICU1:MCU ratio in TA muscles of mice. (D–E) Effects of 5 μg/mL LPS intervention on the components of MCU in C2C12 cells, $n = 3$. (F) Effects of LPS on the MICU1:MCU ratio in C2C12 cells, $n = 3$. (G–H) Gene expression of MCU in mice and C2C12 cells, $n = 3$. Data are shown as mean ± SEM. $^{*}P < 0.05$ compared with the sham group (control group), $^{\blacktriangle}P < 0.05$ compared with the 6-hour intervention group, and $^{\blacklozenge}P < 0.05$ compared with the 12-hour intervention group.

Based on the results of the *in vivo* experiments, we further investigated the effects of LPS on C2C12 cells. The results showed an increase in the expression of MuRF1 and MAFbx after LPS treatment ($P < 0.05$, Figs. 1K–1M). These results suggest that sepsis impairs neuromuscular function, leading to muscle atrophy.

Sepsis reduced the expression of MICU1 and the MICU1:MCU Protein ratio

The results showed that, at CLP-24 h, MICU1 and MICU2 expression decreased, whereas MCU expression increased ($P < 0.05$, Figs. 2A–2B); there was no significant difference in the expression of the EMRE ($P > 0.05$). These results suggest that sepsis alters the expression of mtCU components, which may be a predisposing factor for sepsis-induced skeletal muscle weakness. We then calculated the MICU1:MCU ratio in TA muscles and found that sepsis decreased the MICU1:MCU ratio ($P < 0.05$, Fig. 2C). Furthermore, LPS caused the mtCU in C2C12 cells to exhibit the same changes in protein expression ($P < 0.05$, Figs. 2D–2E) and that LPS intervention reduced the MICU1:MCU ratio ($P < 0.05$, Fig. 2F). Similar results were obtained in all animals ($P < 0.05$, Fig. 2G) and at cellular ($P < 0.05$, Fig. 2H) genetic levels.

LPS disturbed the mitochondrial calcium uptake

To investigate the effects of the LPS-induced decrease in the MICU1:MCU protein ratio on $[Ca^{2+}]_m$ uptake, we detected changes in $[Ca^{2+}]_m$ levels in differentiated mature C2C12 myotube cells after LPS intervention. Hoffman et al. (33) demonstrated that, when $[Ca^{2+}]_c$ levels exceeded 3 μM, the $[Ca^{2+}]_m$ uptake threshold set by MICU1 was overcome, and mitochondria began to take up calcium. Therefore, we explored the sensitivity and extent of MICU1's resistance to calcium loading using different doses of calcium (2.5 and 20 μM) (34). Since we used Tg to exclude the effect of the endoplasmic reticulum on $[Ca^{2+}]_c$ uptake, we continuously monitored $[Ca^{2+}]_c$ with Fluo-4 AM, and changes in fluorescence signal intensity indicated calcium inflow into or out of the mitochondria.

The results showed that, when 2.5 μM of calcium was added, the $[Ca^{2+}]_c$ level increased transiently and the calcium level gradually decreased, indicating that $[Ca^{2+}]_c$ entered the mitochondria. CGP-37157 was subsequently added to inhibit the outflow of $[Ca^{2+}]_m$. The concentration of $[Ca^{2+}]_c$ changed relatively smoothly, indicating that the mitochondria absorbed sufficient calcium. After 6 min, Ru360 was added to inhibit $[Ca^{2+}]_m$ influx by blocking the MCU channels. Finally, FCCP was added to confirm that the increase in $[Ca^{2+}]_c$ was due to $[Ca^{2+}]_m$ release (Fig. 3A) (30).

The amount of calcium in the mitochondria was assessed by calculating the release rate of $[Ca^{2+}]_m$ per unit time after adding FCCP. The results showed that LPS treatment resulted in an accelerated rate of $[Ca^{2+}]_m$ release per unit time ($P < 0.05$, Fig. 3B), indicating that LPS increased levels of calcium in the mitochondrial matrix.

Furthermore, we performed correlation analysis and found that the MICU1:MCU protein ratio was positively correlated with a decrease in the grip strength of mice ($R = 0.6408$, $P = 0.0018$, Fig. 3C). We found that when 2.5 μM of calcium was added, the MICU1:MCU protein ratio was negatively correlated with $[Ca^{2+}]_m$ ($R = 0.8625$, $P < 0.001$, Fig. 3D) (35). These results indicate that LPS decreases the MICU1:MCU ratio, resulting in $[Ca^{2+}]_m$ overload at rest and inducing skeletal muscle dysfunction.

To investigate whether LPS affects the co-activation of MICU1 and MICU2, we used 20 μM of calcium, which was well above the $[Ca^{2+}]_m$ uptake threshold at LPS-24 h, to detect $[Ca^{2+}]_m$ uptake. Similarly, we continuously and dynamically monitored

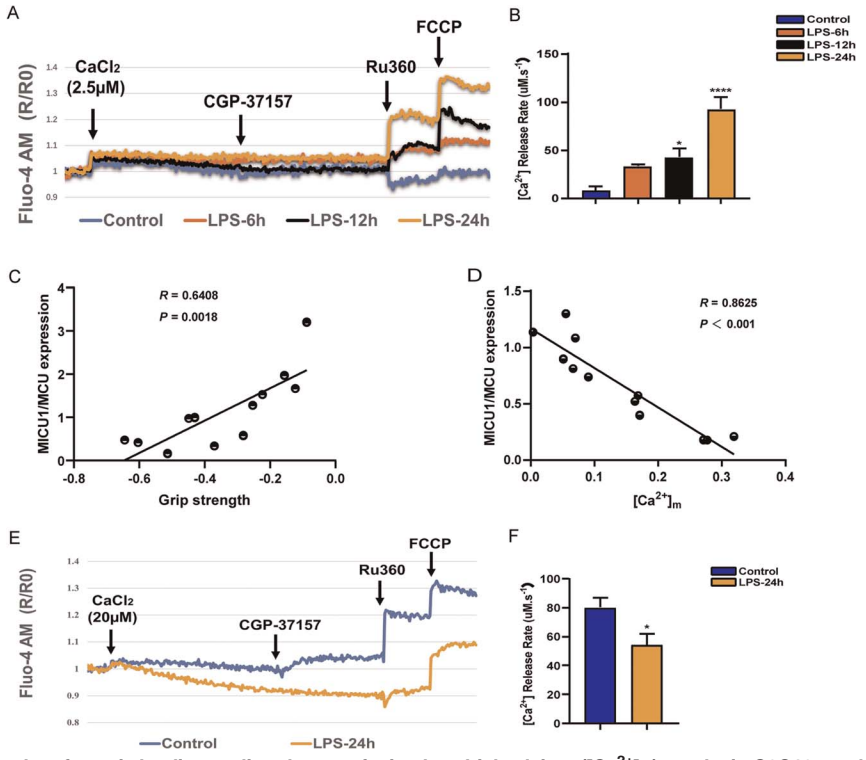

Fig. 3. **Representative line plot of sepsis leading to disturbance of mitochondrial calcium ($[Ca^{2+}]_m$) uptake in C2C12 myoblasts.** (A–B and E–F) $[Ca^{2+}]_m$ uptake and efflux in C2C12 cells after the addition of 2.5 and 20 μM of calcium and $[Ca^{2+}]_m$ release rate at different time groups (three replicates per group). CGP-37157: mitochondrial Na^+-Ca^{2+} channel inhibitor, Ru360: MCU inhibitor, FCCP: mitochondrial uncoupling agent. R/R0 indicates the ratio of each time point to the average base value over the initial 1 min, $n = 6$. (C) Correlation analysis between the MICU1:MCU protein ratio and grip strength in mice after CLP modeling. The X-axis represents grip strength, and the Y-axis represents the MICU1:MCU protein ratio. (D) Correlation analysis between $[Ca^{2+}]_m$ and the MICU1:MCU protein ratio adding 2.5 μM of calcium following LPS intervention in C2C12 cells. The X-axis represents $[Ca^{2+}]_m$, and the Y-axis represents the MICU1:MCU protein ratio. Individual data points are shown with 95% confidence intervals and linear regression. Data are shown as mean ± SEM. *$P < 0.05$ compared with the control group, ▲$P < 0.05$ compared with the LPS-6 h group, and ●$P < 0.05$ compared with the LPS-12 h group.

the changes in $[Ca^{2+}]_c$ concentration by adding different blockers (Fig. 3E). The results showed that, after adding 20 μM of calcium, the mitochondria in the control group released more calcium ($P < 0.05$, Fig. 3F), whereas LPS impaired the co-activation function between MICU1 and MICU2 by reducing the expression of MICU1, resulting in hindered $[Ca^{2+}]_m$ uptake.

MICU1 overexpression improved sepsis-induced skeletal muscle weakness

To explore the role of the MICU1:MCU ratio in sepsis-induced skeletal muscle weakness, we prophylactically overexpressed MICU1 by injecting AAV into the TA muscles of mice ($P < 0.05$, Figs. 4A–4C). We subsequently examined CMAP in mice, and the results showed that the AAV-C-CLP group had impaired CMAP compared with the AAV-C-Sham group ($P < 0.05$). MICU1 overexpression improved skeletal muscle function by increasing CMAP amplitude and decreasing duration and latency ($P < 0.05$, Figs. 4D–4G). Surprisingly, after MICU1 overexpression, the CMAP results of the AAV-M-CLP group were consistent with those of the AAV-C-Sham group ($P > 0.05$). We also examined the expression level of the MICU1:MCU ratio in the TA muscles following AAV administration (Figs. 4H–4J). The results showed that the protein expression of the MICU1:MCU ratio in the AAV-C-CLP group was lower than that in the AAV-C-Sham group ($P < 0.05$). Compared with the AAV-C-CLP group, protein expression of the MICU1:MCU ratio was increased in the AAV-M-CLP group ($P < 0.05$). These results suggest that an increased MICU1:MCU protein ratio reverses sepsis-induced skeletal muscle weakness.

MICU1 overexpression alleviates muscle fiber atrophy

To explore the effects of MICU1 overexpression on skeletal muscle morphology, we used H&E staining to determine the CSA of AAV-infected TA muscles. The results showed that the CSA of TA muscle fibers decreased in the AAV-C-CLP group ($P < 0.05$) but increased in the AAV-M-CLP group after MICU1 overexpression ($P < 0.05$, Figs. 5A–5B). In addition, our results showed that MuRF1 and MAFbx expression increased in the AAV-C-CLP group ($P < 0.05$), whereas MICU1 overexpression decreased MuRF1 and MAFbx expression in the AAV-M-CLP group ($P < 0.05$, Figs. 5C–5E).

Similarly, MICU1 was successfully overexpressed in C2C12 cells infected with LV ($P < 0.05$, Figs. 5F–5H). Consistent with the animal results, LPS increased the expression of MuRF1 and MAFbx in the LV-C-LPS group ($P < 0.05$), whereas MICU1 overexpression decreased the expression of these two atrophy-related proteins in the LV-M-LPS group ($P < 0.05$, Figs. 5I–5K). These results suggest that MICU1 overexpression alleviates sepsis-induced skeletal muscle fiber atrophy.

MICU1 overexpression reverses mitochondrial calcium uptake disorder

To explore the effects of MICU1 prophylactic overexpression on $[Ca^{2+}]_m$ uptake, we continuously and dynamically monitored

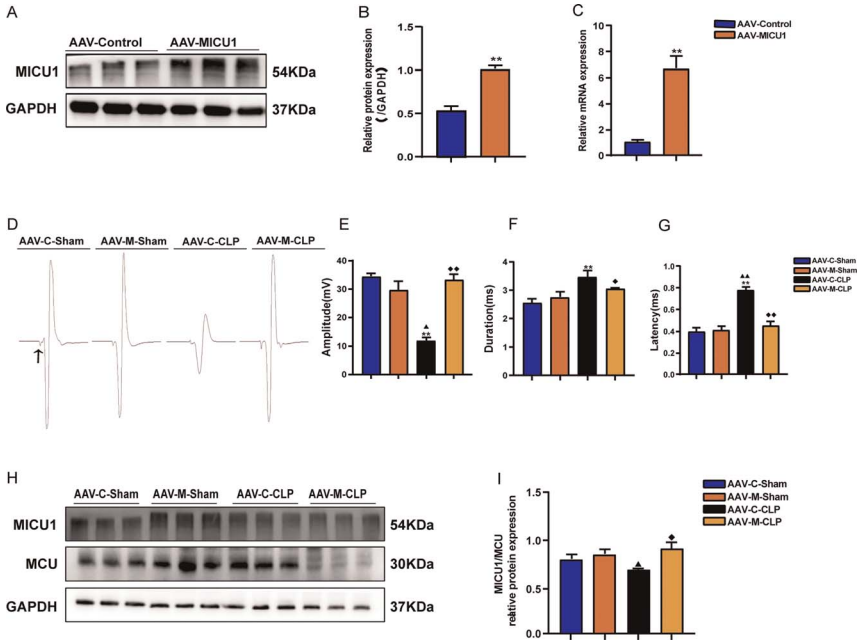

FIG. 4. **MICU1 overexpression improved sepsis-induced skeletal muscle weakness.** (A–C) Representative Western blotting of successful overexpression of MICU1 in tibialis anterior (TA) muscles and statistical analysis of proteins and genes, $n = 3$. (D–G) Representative images of the compound muscle action potential (CMAP) in each group along with three main parameters: amplitude, duration, and latency, $n = 5$. (H–J) The MICU1:MCU protein ratio after MICU1 overexpression in TA muscles, $n = 3$. Data are shown as the mean ± SEM. $^{*}P < 0.05$ compared with the AAV-C-Sham group, $^{\blacktriangle}P < 0.05$ compared with the AAV-M-Sham group, and $^{\blacklozenge}P < 0.05$ compared with the AAV-C-CLP group.

changes in $[Ca^{2+}]_c$ levels on well-differentiated and mature C2C12 myotubes after LV infection. The results showed that, after adding 2.5 μM of calcium, the amount of calcium released by the mitochondria in the LV-C-LPS 24 h group exceeded that in the LV-C-Control group ($P < 0.05$, Figs. 6A–6B), indicating that LPS causes $[Ca^{2+}]_m$ overload in the resting state. However, the $[Ca^{2+}]_m$ release rate decreased in the LV-M-LPS 24 h group after MICU1 overexpression ($P < 0.05$), indicating that $[Ca^{2+}]_m$ overload was alleviated. These results showed that MICU1 overexpression counteracted the effects of LPS, allowing MICU1 to function as a "gatekeeper."

Next, we measured the MICU1:MCU ratio after LV infection in C2C12 cells. The results showed that the MICU1:MCU ratio

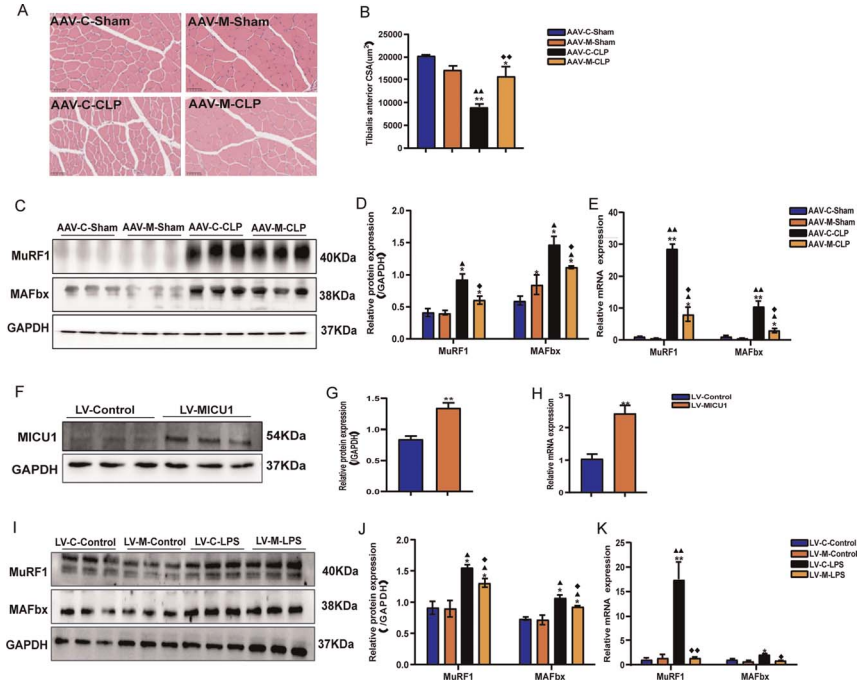

FIG. 5. **Effects of MICU1 overexpression on muscle atrophy in mice and C2C12 cells.** (A–B) Representative hematoxylin and eosin–stained tibialis anterior (TA) muscles (scale bar = 50 μm) and cross-sectional areas of TA muscles, $n = 5$. (C–E) Effects of MICU1 overexpression in mice TA muscles on the expression of MuRF1 and MAFbx, $n = 3$. (F–H) Representative Western blotting of successful overexpression of MICU1 in C2C12 cells and statistical results of proteins and genes, $n = 3$. (I–K) Effects of MICU1 overexpression in C2C12 cells on the expression of MuRF1 and MAFbx, $n = 3$. The data are shown as mean ± SEM. $^{*}P < 0.05$ compared with the AAV-C-Sham (LV-C-Control) group, $^{\blacktriangle}P < 0.05$ compared with the AAV-M-Sham (LV-M-Control) group, and $^{\blacklozenge}P < 0.05$ compared with the AAV-C-CLP (LV-C-LPS) group.

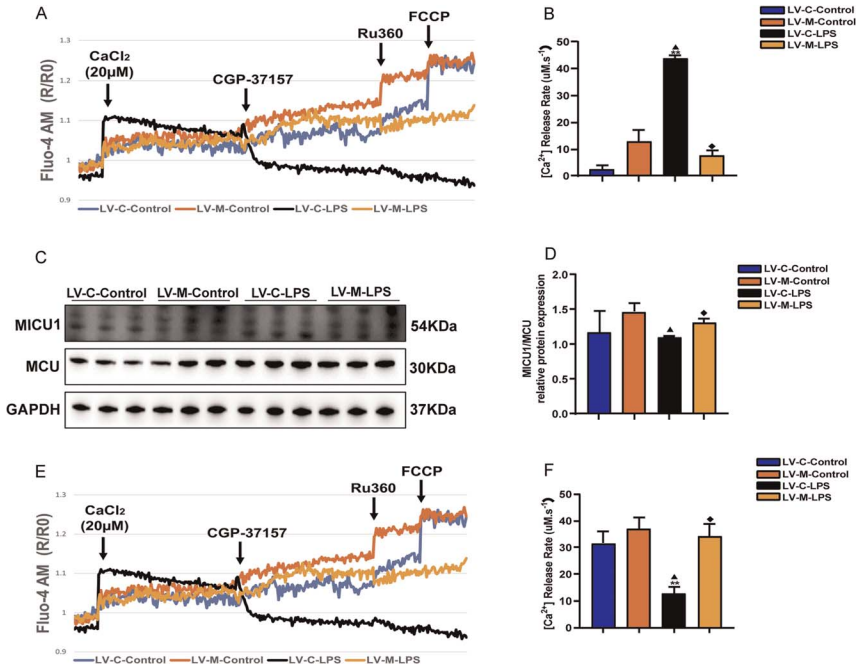

Fig. 6. **MICU1 overexpression reverses sepsis-induced $[Ca^{2+}]_m$ uptake disorders.** (A–B and E–F) $[Ca^{2+}]_m$ uptake and efflux in C2C12 cells after the addition of 2.5 and 20 μM calcium, and the $[Ca^{2+}]_m$ release rate at different time groups (three replicates per group). CGP-37157: mitochondrial Na^+-Ca^{2+} channel inhibitor, Ru360: MCU inhibitor, FCCP: mitochondrial uncoupling agent. R/R0 indicates the ratio of each time point to the average base value over the initial 1 min, $n = 6$. (C–D) The MICU1:MCU protein ratio after MICU1 overexpression in C2C12 cells, $n = 3$. Data are shown as mean ± SEM. $^*P < 0.05$ compared with the LV-C-Control group, $^▲P < 0.05$ compared with the LV-M-Control group, and $^●P < 0.05$ compared with the LV-C-LPS group.

decreased in the LV-C-LPS group compared with the LV-C-Control group ($P < 0.05$, Figs. 6C–6D). Compared with the LV-C-LPS group, the MICU1:MCU protein ratio in the LV-M-LPS group increased ($P < 0.05$). These results suggest that LPS leads to $[Ca^{2+}]_m$ overload at rest by reducing the MICU1:MCU protein ratio.

Similarly, we measured the uptake of $[Ca^{2+}]_m$ after adding 20 μM of calcium. The results showed that the synergistic activation of MICU1 and MICU2 in the LV-C-LPS group was impaired compared with that in the LV-C-Control group ($P < 0.05$, Figs. 6E–6F), which was manifested by the inability of mitochondria to absorb calcium normally. However, MICU1 prophylactic overexpression significantly counteracted the effects of LPS, which were manifested by the rapid uptake of calcium by mitochondria when $[Ca^{2+}]_c$ exceeded the threshold. These results indicate that MICU1 overexpression alleviates LPS-induced $[Ca^{2+}]_m$ uptake disorders.

The survival rate, weight loss, and detection of inflammatory factors are shown in Supplemental Figure 1, http://links.lww.com/SHK/B767, and the mechanism diagram of this study is shown in Figure 7.

DISCUSSION

Skeletal muscles are important target tissues for sepsis and can affect the limbs and respiratory muscles, eventually causing muscle weakness and fiber atrophy (36,37). Approximately 60%–100% of patients with sepsis eventually develop ICUAW, and mortality is high due to the effects of sepsis and sepsis-induced muscle weakness (3,38). The underlying pathophysiology of sepsis is complex and has not yet been fully elucidated.

Mitochondria play key roles in many processes, including cell signaling and the modulation of $[Ca^{2+}]_c$ levels, and influence the activation of cell death pathways (39,40). Disorders in $[Ca^{2+}]_m$ uptake and mitochondrial dysfunction are characteristics of ICUAW (41). Mitochondria are one of the largest calcium pools in skeletal muscle, and the mitochondrial matrix absorbs $[Ca^{2+}]_c$. Calcium serves as a crucial intracellular second messenger that plays a key role in skeletal muscle contractility. During a stage not

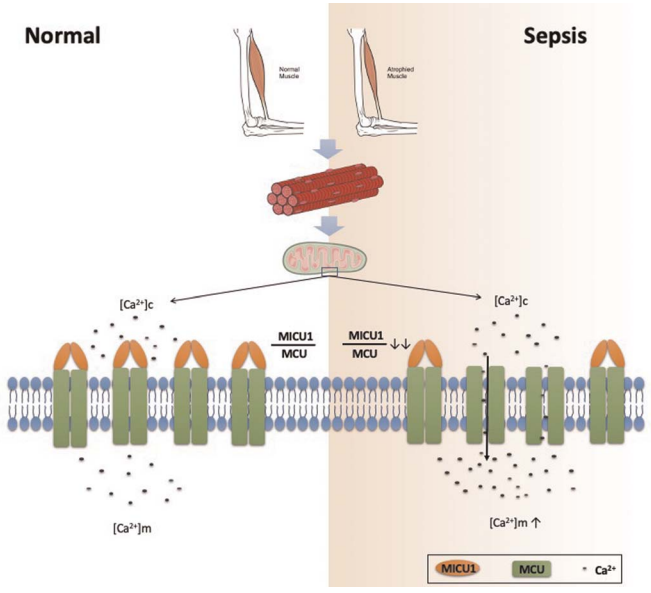

Fig. 7. **Mechanism diagram of this article.** Under physiological conditions, MICU1:MCU maintains normal $[Ca^{2+}]_m$ uptake up to a specific protein ratio. However, sepsis decreases the MICU1:MCU protein ratio, leading to $[Ca^{2+}]_m$ overload and muscle atrophy.

deleterious to myofiber survival, increased $[Ca^{2+}]_m$ uptake stimulates tricarboxylic acid cycling, thereby facilitating energy production during repetitive tetanic contractions. However, $[Ca^{2+}]_m$ overload is an upstream event in mitochondrial depolarization (42). The accumulation of $[Ca^{2+}]_c$ was observed at sites of exercise-induced skeletal muscle damage (43). The function of skeletal muscle is tightly dependent on $[Ca^{2+}]_m$, and $[Ca^{2+}]_m$ overload can trigger permeability transition pore opening, which induces the release of death factors and can lead to myofiber death (44,45). In Duchenne muscular dystrophy, membrane leakage causes calcium to enter mitochondria, eventually leading to $[Ca^{2+}]_m$ overload (46). Therefore, abnormal calcium handling may lead to skeletal muscle dysfunction and mitochondrial involvement (47). $[Ca^{2+}]_m$ uptake is instrumental in cellular physiological and pathophysiological conditions, and impaired $[Ca^{2+}]_m$ uptake may be an important mechanism in ICUAW.

This study found that sepsis decreased MICU1 and MICU2 expression and increased MCU expression, whereas no effect was observed on EMRE, which was identified as a mitochondrial matrix calcium sensor (16). Although Bhosale's results showed that the loss of MICU1 did not affect MCU expression, EMRE expression decreased (48). Given the premise of sepsis, we suspect that the diverse trends in each protein may involve different triggering mechanisms and related factors. The lack of MICU1 considerably affects normal skeletal physiology (18). Consistent with our results, sepsis induces muscle fiber atrophy by decreasing MICU1 expression. However, the upregulation of MCU can trigger muscle hypertrophy through the PGC-1α4 and IGF-Akt/PKB pathways (49). Research has shown that some pathways are activated or inhibited to counteract muscle wasting during muscle atrophy (50). Hence, we suspect that MICU1, in parallel with other pathways, directly promotes muscle wasting and plays a greater role in sepsis-induced skeletal muscle weakness, as well as masking the muscle hypertrophy effect of MCU overexpression. Furthermore, we found that sepsis decreased the expression of MICU2, which plays a critical role in tuning the activity of MICU1 because its EF hands have a low Ca^{2+} binding affinity (18,51). Similar experimental results were also presented by Debattisti et al. (16), who found that knockdown or re-expression of MICU2 was consistent with MICU1 loss. It indicated that MICU2 was not a dominant gatekeeping mechanism and that MICU1 alone was able to accomplish the same function as the MICU1/2 heterodimer.

The "threshold" concept has been widely used to describe the MICU1 gating behavior, and MICU1 is the most important regulator of $[Ca^{2+}]_m$ internal flow (52). Depending on the $[Ca^{2+}]_c$ concentration, MICU1 has two opposite effects: channel inhibition at low $[Ca^{2+}]_c$ levels and a dominant role in channel activation when the concentration of $[Ca^{2+}]_c$ is high (16). Previous studies have shown that loss-of-function mutations in MICU1 cause dysregulation of $[Ca^{2+}]_m$ uptake, leading to brain and muscle disorders (15). To study the dynamic changes in $[Ca^{2+}]_m$ uptake, we indirectly detected $[Ca^{2+}]_c$ in differentiated mature C2C12 myotube cells and found that LPS impaired $[Ca^{2+}]_m$ uptake. By transfecting C2C12 cells with an LV to prophylactically overexpress MICU1, we found that $[Ca^{2+}]_m$ uptake disorders could be significantly alleviated. Low $[Ca^{2+}]_c$ levels were sufficient to trigger an increase in $[Ca^{2+}]_m$ levels after MCU overexpression and MICU1 silencing, and neither MICU3 nor EMRE participated in the tissue-specific calcium dependence of the mtCU (17).

In our experiments, LPS increased MCU expression and decreased MICU1 expression, which caused $[Ca^{2+}]_m$ overload in the resting state. However, discussing the effects of both separately on $[Ca^{2+}]_m$ uptake in skeletal muscle is one-sided, given that different tissues, including skeletal muscle, express different quantities of MICU1 and MCU and that variations in $[Ca^{2+}]_m$ uptake properties among these tissues may be attributed to alterations in the MICU1:MCU protein ratio (18). Therefore, we calculated the protein ratio of MICU1 to MCU to accurately explore the influx of $[Ca^{2+}]_m$ and found that sepsis decreased the MICU1:MCU protein ratio, resulting in $[Ca^{2+}]_m$ overload and skeletal muscle atrophy (Fig. 7).

There are two major limitations in this study that could be addressed in our future research. First, in animal experiments, CLP was used to induce mouse models of sepsis, and antibiotics were not used. It was reported that antibiotics would affect cellular metabolism and mitochondrial function (53). Therefore, to exclude the effects of antibiotics on mitochondrial function and age-related sarcopenia, we carried out the study in adult mice and did not treat them with antibiotic agents, which resulted in experimental bias due to high mortality. Second, in the section on cell experiments, LPS was used to induce inflammation in differentiated C2C12 myoblasts. LPS is a substance found in gram-negative bacteria, and it cannot mimic the pathophysiological changes of patients with sepsis caused by polymicrobial infections. Our subsequent studies will further explore the effects of other pathogenic bacteria on skeletal muscle mitochondrial function.

In conclusion, our results demonstrated that sepsis-induced skeletal muscle weakness and atrophy are associated with impaired $[Ca^{2+}]_m$ uptake caused by a decreased MICU1:MCU protein ratio.

ACKNOWLEDGMENTS

The authors would like to thank Editage (www.editage.cn) for English language editing.

REFERENCES

1. Yang T, Li Z, Jiang L, et al. Hyperlactacidemia as a risk factor for intensive care unit–acquired weakness in critically ill adult patients. *Muscle Nerve*. 2021;64(1):77–82.
2. Zanders L, Kny M, Hahn A, et al. Sepsis induces interleukin 6, gp130/JAK2/STAT3, and muscle wasting. *J Cachexia Sarcopenia Muscle*. 2022;13(1):713–727.
3. Haberecht-Müller S, Krüger E, Fielitz J. Out of control: the role of the ubiquitin proteasome system in skeletal muscle during inflammation. *Biomolecules*. 2021;11(9):1327.
4. Raurell-Torredà M, Arias-Rivera S, Martí JD, et al. Care and treatments related to intensive care unit–acquired muscle weakness: a cohort study. *Aust Crit Care*. 2021;34(5):435–445.
5. Li Z, Zhang Q, Zhang P, et al. Prevalence and risk factors for intensive care unit acquired weakness: a protocol for a systematic review and meta-analysis. *Medicine*. 2020;99(36):e22013.
6. Boelens YFN, Melchers M, Van Zanten ARH. Poor physical recovery after critical illness: incidence, features, risk factors, pathophysiology, and evidence-based therapies. *Curr Opin Crit Care*. 2022;28(4):409–416.
7. Yang Z, Wang X, Wang F, et al. A systematic review and meta-analysis of risk factors for intensive care unit acquired weakness. *Medicine*. 2022;101(43):e31405.
8. Klawitter F, Ehler J, Bajorat R, et al. Mitochondrial dysfunction in intensive care unit–acquired weakness and critical illness myopathy: a narrative review. *Int J Mol Sci*. 2023;24(6):5516.
9. Maestraggi Q, Lebas B, Clere-Jehl R, et al. Skeletal muscle and lymphocyte mitochondrial dysfunctions in septic shock trigger ICU-acquired weakness and sepsis-induced immunoparalysis. *Biomed Res Int*. 2017;2017:1–12.

10. Tomar D, Elrod JW. Metabolite regulation of the mitochondrial calcium uniporter channel. *Cell Calcium*. 2020;92:102288.
11. Márta K, Hasan P, Rodríguez-Prados M, et al. Pharmacological inhibition of the mitochondrial Ca^{2+} uniporter: relevance for pathophysiology and human therapy. *J Mol Cell Cardiol*. 2021;151:135–144.
12. Wang C, Jacewicz A, Delgado BD, et al. Structures reveal gatekeeping of the mitochondrial Ca^{2+} uniporter by MICU1-MICU2. *Elife*. 2020;9:e59991.
13. Wu W, Shen Q, Zhang R, et al. The structure of the MICU 1- MICU 2 complex unveils the regulation of the mitochondrial calcium uniporter. *EMBO J*. 2020;39(19).
14. Kohlschmidt N, Elbracht M, Czech A, et al. Molecular pathophysiology of human MICU1 deficiency. *Neuropathol Appl Neurobiol*. 2021;47(6):840–855.
15. Logan CV, Szabadkai G, Sharpe JA, et al. Loss-of-function mutations in MICU1 cause a brain and muscle disorder linked to primary alterations in mitochondrial calcium signaling. *Nat Genet*. 2014;46(2):188–193.
16. Debattisti V, Horn A, Singh R, et al. Dysregulation of mitochondrial Ca^{2+} uptake and sarcolemma repair underlie muscle weakness and wasting in patients and mice lacking MICU1. *Cell Reports*. 2019;29(5):1274–1286.e6.
17. Paillard M, Csordás G, Szanda G, et al. Tissue-specific mitochondrial decoding of cytoplasmic Ca^{2+} signals is controlled by the stoichiometry of MICU1/2 and MCU. *Cell Rep*. 2017;18(10):2291–2300.
18. Tsai C-W, Rodriguez MX, Van Keuren AM, et al. Mechanisms and significance of tissue-specific MICU regulation of the mitochondrial calcium uniporter complex. *Mol Cell*. 2022;82(19):3661–3676.e8.
19. Shanmughapriya S, Tomar D, Dong Z, et al. FOXD1-dependent MICU1 expression regulates mitochondrial activity and cell differentiation. *Nat Commun*. 2018;9(1):3449.
20. Drechsler S, Osuchowski M. Cecal ligation and puncture. In: Walker WE, ed. *Sepsis. Methods in Molecular Biology*. 2321. New York, NY: Springer US; 2021:1–8.
21. Tsuchida T, Wada T, Mizugaki A, et al. Protocol for a sepsis model utilizing fecal suspension in mice: fecal suspension intraperitoneal injection model. *Front Med*. 2022;9:765805.
22. Alverdy JC, Keskey R, Thewissen R. Can the cecal ligation and puncture model be repurposed to better inform therapy in human sepsis? *Infect Immun*. 2020;88(9): e00942–e00919.
23. Hellman J, Bahrami S, Boros M, et al. Part III: minimum quality threshold in preclinical sepsis studies (MQTiPSS) for fluid resuscitation and antimicrobial therapy endpoints. *Shock*. 2019;51(1):33–43.
24. Yang X, Xue P, Liu Z, et al. SESN2 prevents the slow-to-fast myofiber shift in denervated atrophy via AMPK/PGC-1α pathway. *Cell Mol Biol Lett*. 2022;27(1):66. doi:10.1186/s11658-022-00367-z.
25. Yu Z, Zhang M, Jing H, et al. Characterization of LRP4/Agrin antibodies from a patient with myasthenia gravis. *Neurology*. 2021;97(10):e975–e987.
26. Pollari E, Prior R, Robberecht W, et al. In vivo electrophysiological measurement of compound muscle action potential from the forelimbs in mouse models of motor neuron degeneration. *J Vis Exp*. 2018;136:57741.
27. Vilar-Pereira G, de Souza Ruivo LA, Lannes-Vieira J. Behavioural alterations are independent of sickness behaviour in chronic experimental Chagas disease. *Mem Inst Oswaldo Cruz*. 2015;110(8):1042–1050.
28. Zhao Y, Shen F, Gong M, et al. Lifelong treadmill training improves muscle function detected by a modified grip strength test during aging in BALB/c mice. *Life Sci*. 2020;251:117603.
29. Brearley-Sholto MC, Loczenski-Brown DM, Jones S, et al. Effect of AAV-mediated overexpression of ATF5 and downstream targets of an integrated stress response in murine skeletal muscle. *Sci Rep*. 2021;11:19796.
30. Mallilankaraman K, Doonan P, Cárdenas C, et al. MICU1 is an essential gatekeeper for MCU-mediated mitochondrial Ca^{2+} uptake that regulates cell survival. *Cell*. 2012;151(3):630–644.
31. Zhou Q, Xie M, Zhu J, et al. PINK1 contained in huMSC-derived exosomes prevents cardiomyocyte mitochondrial calcium overload in sepsis via recovery of mitochondrial Ca^{2+} efflux. *Stem Cell Res Ther*. 2021;12(1):269.
32. Liu Z, Zhang Z, Song G, et al. Resveratrol alleviates skeletal muscle insulin resistance by downregulating long noncoding RNA. *Int J Endocrinol*. 2022;2022: 2539519.
33. Hoffman NE, Chandramoorthy HC, Shamugapriya S, et al. MICU1 motifs define mitochondrial calcium uniporter binding and activity. *Cell Rep*. 2013;5(6):1576–1588.
34. Stoll S, Xi J, Ma B, et al. The Valosin-containing protein protects the heart against pathological Ca^{2+} overload by modulating Ca^{2+} uptake proteins. *Toxicol Sci*. 2019; 171(2):473–484.
35. Schober P, Boer C, Schwarte LA. Correlation coefficients: appropriate use and interpretation. *Anesth Analg*. 2018;126(5):1763–1768.
36. Vankrunkelsven W, Derde S, Gunst J, et al. Obesity attenuates inflammation, protein catabolism, dyslipidaemia, and muscle weakness during sepsis, independent of leptin. *J Cachexia Sarcopenia Muscle*. 2022;13(1):418–433.
37. Leduc-Gaudet JP, Mayaki D, Reynaud O, et al. Parkin overexpression attenuates sepsis-induced muscle wasting. *Cell*. 2020;9(6):1454.
38. Cao Y, Wang Z, Yu T, et al. Sepsis induces muscle atrophy by inhibiting proliferation and promoting apoptosis via PLK1-AKT signalling. *J Cell Mol Med*. 2021; 25(20):9724–9739.
39. Hood DA, Memme JM, Oliveira AN, et al. Maintenance of skeletal muscle mitochondria in health, exercise, and aging. *Annu Rev Physiol*. 2019;81(1):19–41.
40. Annesley SJ, Fisher PR. Mitochondria in health and disease. *Cell*. 2019;8(7):680.
41. Iepsen UW, Plovsing RR, Tjelle K, et al. The role of lactate in sepsis and COVID-19: perspective from contracting skeletal muscle metabolism. *Exp Physiol*. 2022; 107(7):665–673.
42. Kostic M, Ludtmann MHR, Bading H, et al. PKA phosphorylation of NCLX reverses mitochondrial calcium overload and depolarization, promoting survival of PINK1-deficient dopaminergic neurons. *Cell Rep*. 2015;13(2):376–386.
43. Roman W, Pinheiro H, Pimentel MR, et al. Muscle repair after physiological damage relies on nuclear migration for cellular reconstruction. *Science*. 2021; 374(6565):355–359.
44. Robichaux DJ, Harata M, Murphy E, et al. Mitochondrial permeability transition pore-dependent necrosis. *J Mol Cell Cardiol*. 2023;174:47–55.
45. Agrawal A, Suryakumar G, Rathor R. Role of defective Ca^{2+} signaling in skeletal muscle weakness: pharmacological implications. *J Cell Commun Signal*. 2018; 12(4):645–659.
46. Zabłocka B, Górecki DC, Zabłocki K. Disrupted calcium homeostasis in Duchenne muscular dystrophy: a common mechanism behind diverse consequences. *Int J Mol Sci*. 2021;22(20):11040.
47. Billingham LK, Stoolman JS, Vasan K, et al. Mitochondrial electron transport chain is necessary for NLRP3 inflammasome activation. *Nat Immunol*. 2022;23(5):692–704.
48. Bhosale G, Sharpe JA, Koh A, et al. Pathological consequences of MICU1 mutations on mitochondrial calcium signalling and bioenergetics. *Biochim Biophys Acta Mol Cell Res*. 2017;1864(6):1009–1017.
49. Mammucari C, Gherardi G, Zamparo I, et al. The mitochondrial calcium uniporter controls skeletal muscle Trophism in vivo. *Cell Rep*. 2015;10(8):1269–1279.
50. Butera G, Vecellio Reane D, Canato M, et al. Parvalbumin affects skeletal muscle trophism through modulation of mitochondrial calcium uptake. *Cell Rep*. 2021; 35(5):109087.
51. Kamer KJ, Jiang W, Kaushik VK, et al. Crystal structure of MICU2 and comparison with MICU1 reveal insights into the uniporter gating mechanism. *Proc Natl Acad Sci U S A*. 2019;116(9):3546–3555.
52. Park J, Lee Y, Park T, et al. Structure of the MICU1–MICU2 heterodimer provides insights into the gatekeeping threshold shift. *IUCrJ*. 2020;7(2):355–365.
53. Singh R, Sripada L, Singh R. Side effects of antibiotics during bacterial infection: mitochondria, the main target in host cell. *Mitochondrion*. 2014;16:50–54.